buildings

MDPI

Article

Modelling of Strengthened Steel Connections under Static and Cyclic Loading

Mourad Khelifa [1,*], Amar Khennane [2] and Marc Oudjene [3]

1 EA 4370, LERMAB, University of Lorraine, 27 Rue Philippe SÉGUIN, 88051 Épinal, France
2 SEIT, UNSW Canberra, Northcott Drive, Campbell, ACT 2600, Australia
3 Department of Civil Engineering and Water Engineering, University of Laval, 1065 Avenue de la Médecine, Québec, QC G1V 0A6, Canada
* Correspondence: mourad.khelifa@univ-lorraine.fr; Tel.: +33-(0)3-72-74-96-18

Abstract: The rehabilitation of steel structures with Fibre Reinforced Polymers (FRP's) may appear less effective because they can be bolted or welded with steel plates that display the same mechanical properties. However, this technique has some unwanted consequences such as additional dead weight and an increased risk of corrosion. The aim of the proposed study, therefore, is to present a technique for modelling steel connections strengthened with FRP's. Two types of composites: Carbon Fibre Reinforced Polymer (CFRP) and Glass Fibre Reinforced Polymer (GFRP) are considered. They are used to strengthen welded steel connections. The main objective consists in evaluating the effect of the reinforcement on the load-carrying capacity of these connections under monotonic and cyclic loadings. The steel is considered to behave in a linear elastic perfectly plastic fashion with isotropic strain hardening, and the FRP's are assumed to behave linearly up to failure. The behaviour of the adhesive is modelled with the Cohesive Zone Model (CZM) available in Abaqus. Lastly, a parametric study is carried out to investigate the eventuality of strengthening connections made with I-sections, which are very common in practice.

Keywords: finite element models; steel connections; CFRP; GFRP; Cohesive Zone Model; static and cyclic loading

Citation: Khelifa, M.; Khennane, A.; Oudjene, M. Modelling of Strengthened Steel Connections under Static and Cyclic Loading. *Buildings* **2022**, *12*, 1962. https://doi.org/10.3390/buildings12111962

Academic Editors: Humberto Varum and Bo Yang

Received: 27 August 2022
Accepted: 2 November 2022
Published: 11 November 2022

1. Introduction

The use of structural steel is not only cost-effective but also long lasting. Structural steel offers additional advantages such as robustness, fast construction times, ductility, and ease of recycling. However, it has the disadvantage of being susceptible to corrosion. Besides, steel structures are often subjected to complex stresses such as those induced by overloads, fluctuations in temperature of the surrounding environment, fire, and the effects of cyclic loads whose consequences can be disastrous particularly in seismic areas [1]. Therefore, to increase the service life of these structures, it is advisable to put in place adequate repair and reinforcement techniques [1,2].

In the case of metallic structures, the advantage of reinforcement by fibre reinforced composites may seem less obvious because they can be bolted or welded to similar reinforcing materials with the same mechanical properties. This method, however, does have unwanted consequences such as additional dead weight and increased risk of corrosion. The use of welding is not encouraged either because of the phenomenon of fatigue particularly in the presence of cyclic loading. The alternative, therefore, is to use fibre reinforced polymers (FRP's), a technique that has already proven its effectiveness in restoring the load carrying ability of reinforced concrete and timber structures [3,4]. Other advantages of using FRP's include the ability of such laminates to follow curved surfaces, particularly when the wet lay-up process is used, the reduced disturbance to services and traffic, and the complete absence of residual stresses such as those induced by welding steel plates. This makes them particularly attractive for retrofitting historic metallic structures, because they overcome the non-weldability of certain metals, they do not require the modification of the initial architectural design of the structure, and/or add dead weight to the initial configuration [5–9].

Nowadays, many authors agree on the effectiveness of bonding FRP composites to rehabilitate metallic structures [10,11]. An excellent review on this topic citing 163 references is published in [12]. However, there are still some unanswered questions regarding the durability of the structural bond under service conditions. Indeed, the values of the reduction coefficients proposed in the design codes to account for the environmental degradation of bonded composites are generally not well argued or backed up by research data. Moreover, the codes often justify these values by referring to the degradation of the reinforcing material rather than to the evolution of the bonded interface. Debonding failures are the most challenging issues because the adhesive constitutes the weakest link. In terms of theoretical modelling, a key issue is the strong interaction between debonding and crack propagation in cyclic loading as reported in [12]. Another issue is the accurate prediction of the progressive failure of composite laminates. This has been the subject of several studies [13–17] because of its crucial importance for the development and design of composite structures. Bui TQ and Hu X (2021) in [13] presents a critical analysis of recent developments and applications of regularized phase-field models for failure cases in laminates and composite structures. The phase field model described in [13] considers the cohesive zone model, material plasticity, damage initiation criterion and energy decay. And it is formulated at different microscopic, mesoscopic and macroscopic scales. The approach used in this study is different because it is formulated from the mechanics of continuous media coupled with a cohesive model.

The aim of this study, therefore, is to propose a numerical model to describe the static and cyclic behaviour of steel connections produced by welding and strengthened with composites. Indeed, failures of steel structures are primarily the result of a connection failure. The main objective is to provide technical and numerical tools for practicing engineers to dimension and design connections strengthened by composites under monotonic and cyclic loading. A particular attention is given to the bonded interface. It is modelled using the Cohesive Zone Model (CZM) available in Abaqus [18], which is a very popular computational tool for modelling fracture in engineering materials. A comparison between the rigidities under static and dynamic loading is presented and commented on. Finally, a parametric study on the impact of the length of reinforcement on the bearing capacity of a welded connection commonly used in practice is carried out and discussed.

2. Mechanical Characterisation and Material Properties

2.1. Constitutive Equations

The generalised Hooke's law is written as

$$\underline{\sigma} = \underline{\underline{\Delta}} : \underline{\varepsilon}^e = \underline{\underline{\Delta}} : (\underline{\varepsilon} - \underline{\varepsilon}^p) \tag{1}$$

where $\underline{\sigma}$, $\underline{\varepsilon}$, $\underline{\varepsilon}^e$, $\underline{\varepsilon}^p$ and $\underline{\underline{\Delta}}$ stand respectively for the stress tensor, the total strain, the elastic strain, the plastic strain; and the fourth order tensor of elastic properties.

Inversely, the strain tensor can be written in the isotropic case as follows:

$$\underline{\varepsilon} = \frac{1+\nu}{E}\underline{\sigma} - \frac{\nu}{E} tr(\underline{\sigma})\underline{1} \tag{2}$$

where $\underline{1}$ is the unit tensor of order 2, E the elastic modulus, and ν is Poisson's ratio.

The criterion for plastic flow is described by the loading function f as follows [19]:

$$f = \sqrt{\underline{\sigma} : \underline{\underline{H}} : \underline{\sigma}} - R = \sigma_y - R; \sigma_y = \sqrt{\underline{\sigma} : \underline{\underline{H}} : \underline{\sigma}} \quad \text{and} \quad R = Q\left(1 - e^{-b\bar{\varepsilon}^p}\right) \tag{3}$$

where σ_y is the equivalent stress; Q and b are hardening parameters; $\bar{\varepsilon}^p$ is the equivalent plastic strain; $\underline{\underline{H}}$ is the Hill tensor of order 4 and function of six constants ($F,\ G,\ H,\ L,\ M\ and\ N$) [20]. In the isotropic case, expression (3) reduces to the von Mises criterion with [20]:

$$\underline{\underline{H}} = \begin{bmatrix} G+H & -H & -G & 0 & 0 & 0 \\ -H & H+F & -F & 0 & 0 & 0 \\ -G & -F & F+G & 0 & 0 & 0 \\ 0\ \ 0\ \ 0 & & & 2L & 0 & 0 \\ 0\ \ 0\ \ 0 & & & 0 & 2M & 0 \\ 0\ \ 0\ \ 0 & & & 0 & 0 & 2N \end{bmatrix};\ F = G = H = 0.5\ and\ L = M = N = 1.5 \tag{4}$$

To characterise the mechanical behaviour of steel, it is necessary to determine the two elastic constants (E and ν) and the three plastic constants ($\sigma_y,\ Q$ and b).

2.2. Identification Procedure

The identification of the parameters of the model is detailed in what follows.

(a) Elastic properties

Since steel is considered isotropic, at least in its elastic part, the value of the elastic modulus, $E = 190$ GPa, has been determined from a uniaxial tensile test. The value of Poisson's ratio is taken as equal to $\nu = 0.3$.

(b) Plastic properties

In the case of mono-axial loading, the hardening curve σ_p can be written in the form:

$$\sigma_p = \sigma_y + Q\left(1 - e^{-b\bar{\varepsilon}^p}\right) \tag{5}$$

The parameters to determine are σ_y; Q and b. Knowing the yield strength, one can fix the value of σ_y, and estimate the other two parameters (Q and b) using the method of least squares to express σ_p as a function $\bar{\varepsilon}^p$.

Three tensile tests reported in [2] were used to characterise the mechanical behaviour of the steel. The stress-strain relationship, shown in Figure 1, is fitted to the experimental results using least squares. From a plastic strain $\bar{\varepsilon}^p = 0.2\%$ corresponding to $\sigma_y = 360$ MPa the local stress-strain response becomes non-linear up to $\bar{\varepsilon}^p = 6.12$ % corresponding to $\sigma_y = 472$ MPa. Beyond this limit, the solution remains stable and stationary forming a plateau until a plastic deformation of approximately $\bar{\varepsilon}^p = 20$ % corresponding to $\sigma_y = 478$ MPa.

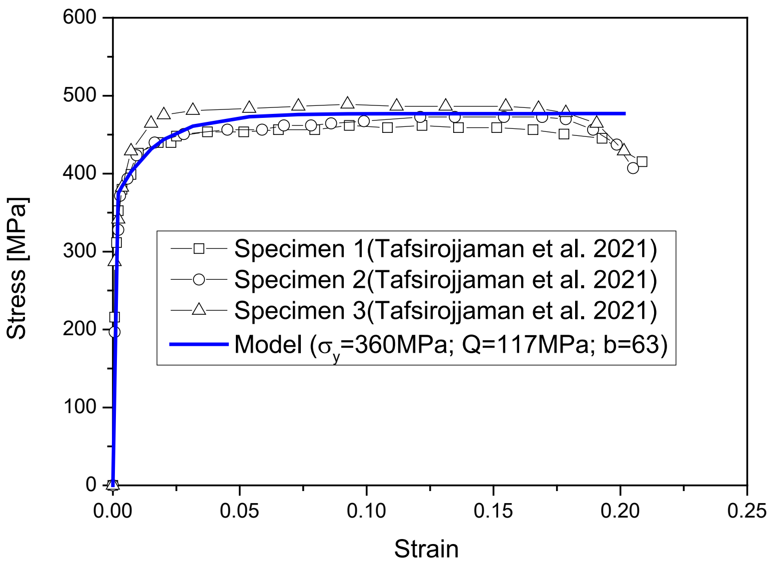

Figure 1. Stress-strain curves for steel [2].

2.3. Cohesive Zone Model CZM

The available Cohesive Zone Model CDM in Abaqus [18] has the shape of a bi-linear curve as shown in Figure 2. First, it considers a linear elastic behaviour followed by softening. The linear elastic behaviour is expressed in terms of an elastic constitutive matrix that relates the normal $\sigma_{0,n}^{I}$ and shear $\sigma_{0,t}^{II}$ stresses to the normal δ_{n}^{I} and shear δ_{t}^{II} separations across the contact interface.

$$\begin{Bmatrix} \sigma_n \\ \sigma_t \end{Bmatrix} = \begin{bmatrix} K_n & 0 \\ 0 & K_t \end{bmatrix} \begin{Bmatrix} \delta_n \\ \delta_t \end{Bmatrix} \tag{6}$$

K_n and K_t are respectively the normal and shear stiffness coefficients.

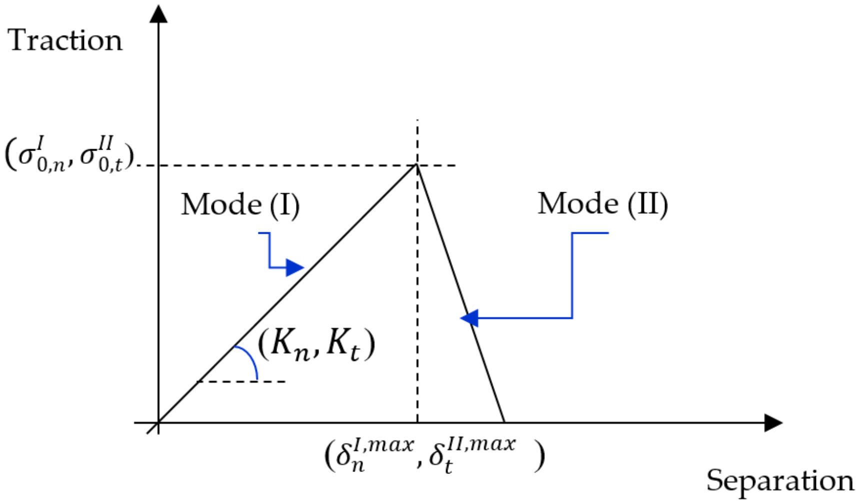

Figure 2. Typical traction-separation response.

All the material properties (steel and cohesive) used in the simulations are summarised in Table 1. The FRP materials are considered linear elastic, and the adhesive is considered to have a maximum stress of 45 MPa, a maximum displacement of 0.01 mm, an initial stiffness of 4500 N/mm^3, and a thickness of 0.06 mm.

Table 1. Material properties.

Steel		FRP		Adhesive (*)
Elasticity	**Plasticity**	**GFRP**	**CFRP**	
$E = 190$ GPa ; $\nu = 0.3$	$\sigma_y = 360$ MPa ; $Q = 117$ MPa; $b = 63$; $F = G = H = 0.5$; $L = M = N = 1.5$	$E = 55$ GPa	$E = 75$ GPa	$\sigma_{max} = 45$ MPa ; $\delta_{max} = 0.01$ mm ; $K_n = 4500$ N/mm^3 ; $t = 0.6$ mm.

(*): σ_{max} is the maximum adhesive strength; δ_{max} is the maximum displacement; K_n is the initial stiffness; t is the thickness of the adhesive.

3. Finite Element Modelling

To develop a finite element model that can be used to run a parametric analysis, it must be first validated using experimental data. The tests presented in [2] are simulated using the same experimental conditions. The connection is formed of Square Hollow Sections (SHS) of dimensions 100 × 100 × 3 mm assembled by welding and strengthened using FRP as shown in Figure 3.

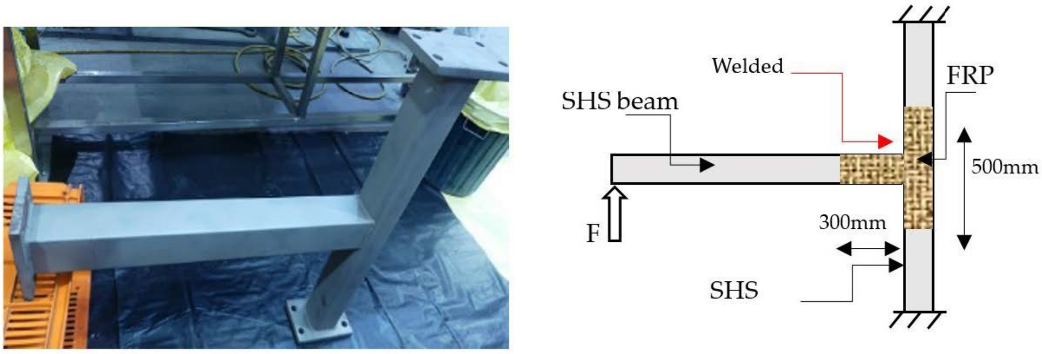

(a) Tested specimen (b) Schematic diagram

Figure 3. Welded steel connections [2].

The finite element model is shown in Figure 4. The two square tubes were meshed with 8000 linear solid elements with 8 nodes of the type C3D8. The FRP is meshed with 3100 quadrilateral 4-node shell elements type S4.

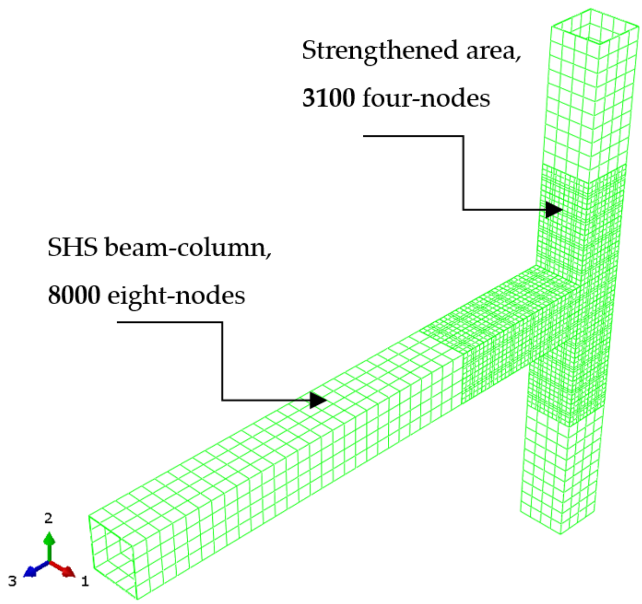

Figure 4. Finite element model.

The behaviour of the adhesive is modelled by the cohesive model available in Abaqus [19]. The adhesive interaction between the steel and the FRP can be accounted for in two ways: either using cohesive elements or through surface-based cohesive behaviour, or to specify the cohesive behaviour between the interacting surfaces. These two methods lead to similar results, but the surface-based cohesive behaviour is easier to use because it does not require meshing the adhesive layer. Further details on the cohesive model are given in [3].

4. Validation

4.1. Under Monotonic Loading

Figure 5 compares the predicted values in terms of force-displacement to the experimental ones. The predicted response is linear up to a vertical displacement u = 6.445 mm corresponding to a force F = 6.705 kN. Beyond this limit, the response becomes non-linear up to a displacement u = 30 mm (F = 17.537 kN). The force measured for the un-strengthened connection at a vertical displacement of 30 mm is approximately equal to 18.148 kN, which corresponds to an error of 3.4% between the predicted and measured values. Figure 5 also shows that the reinforcement improves the mechanical strength of the connection. For the same displacement u = 30 mm, the bearing capacities of the connections strengthened with GFRP and CFRP are respectively equal to 20.843 kN and 23.048 kN, which constitute improvements of respectively 14.85% and 27% compared to the un-strengthened control connection, which again proves the advantage of reinforcing the steel connections with FRP composites.

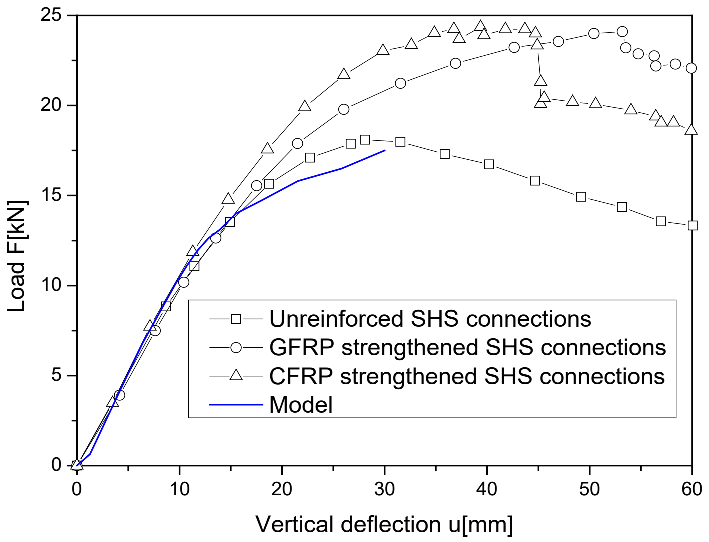

Figure 5. Force displacement curves for the connection under static loading.

Figure 6 shows the distribution of the normal stress σ_z and the von Mises stress at a vertical displacement (u = 30 mm) for the non-strengthened connection under monotonic loading. Figure 6a,b clearly show an area of stress concentration at the junction between the profiles. A clear distinction between the compression and tensile zones can be seen on Figure 6a. The maximum stresses are equal in magnitude but of different sign, which is consistent with the tests, and they are approximately equal to $\sigma_z = 585.8$ MPa. Figure 6b shows that the distribution of the equivalent stress forms a circle at the level of the junction, hence the advantage of reinforcing the connection at this level.

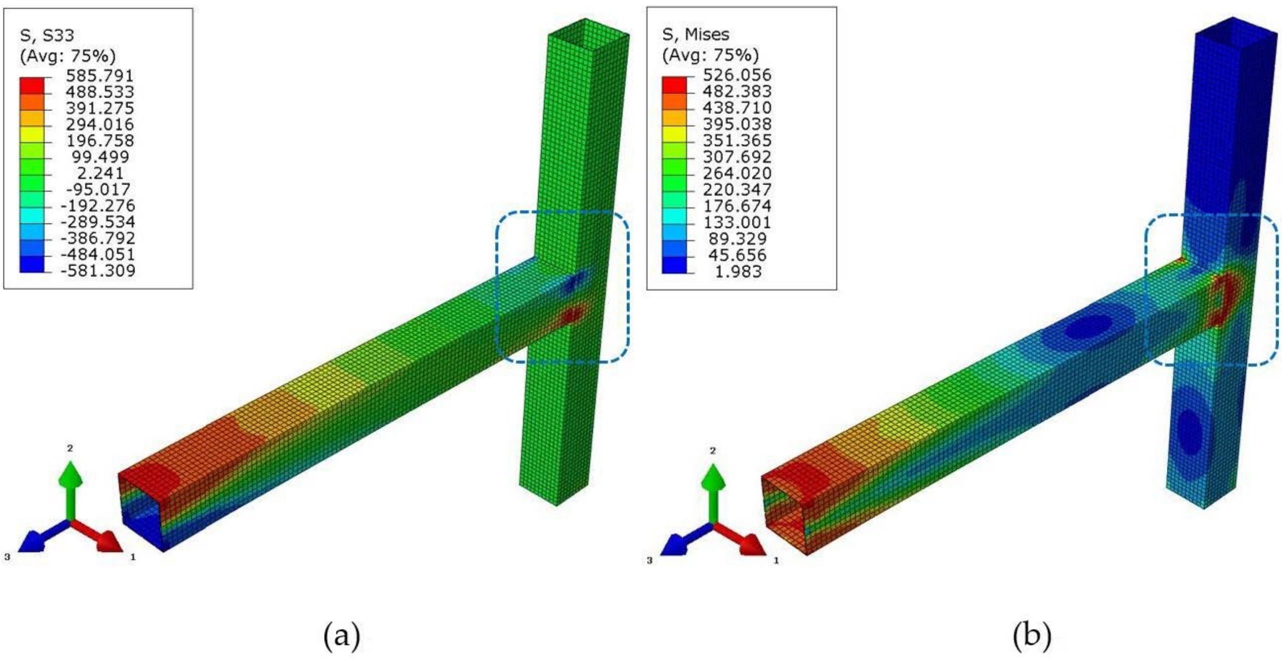

Figure 6. Contour plots for non-strengthened connection: (**a**) σ_z and (**b**) Von-Mises stress.

Figure 7 shows the contour plots of the von Mises stress for the strengthened connection at a vertical displacement (u = 30 mm). It clearly displays an area of stress concentration in the beam-to-column junction. The stress reached is approximately $\sigma_y = 828.1$ MPa, which exceeds that of steel. In this case, it is the reinforcing fibres that take up the tensile forces.

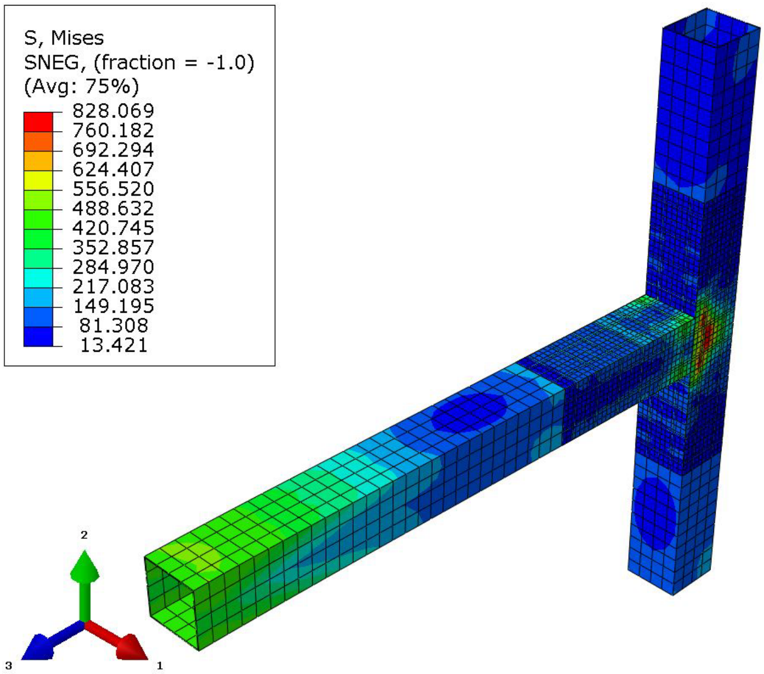

Figure 7. Contour plot of the Von-Mises for the CFRP strengthened connection.

The results of the simulation presented in Figure 8 also show the advantages of reinforcing steel connections with FRP.

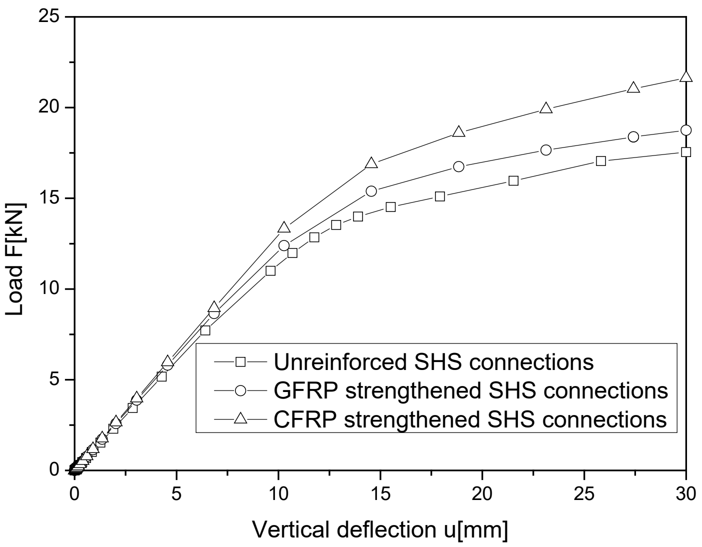

Figure 8. Simulated force displacement curves for the connection under static loading.

The reinforcement also improves the rigidity of the connection as shown in Figures 8 and 9. The initial stiffnesses of the strengthened and un-strengthened systems are constant up to a vertical displacement of u = 6.445 mm, beyond which they begin to decrease gradually. The calculated initial stiffness values are K = 1202.1 kN/m for the control, 1265.4 kN/m for the GFRP strengthened connection, and 1298.2 kN/m the CFRP strengthened connection.

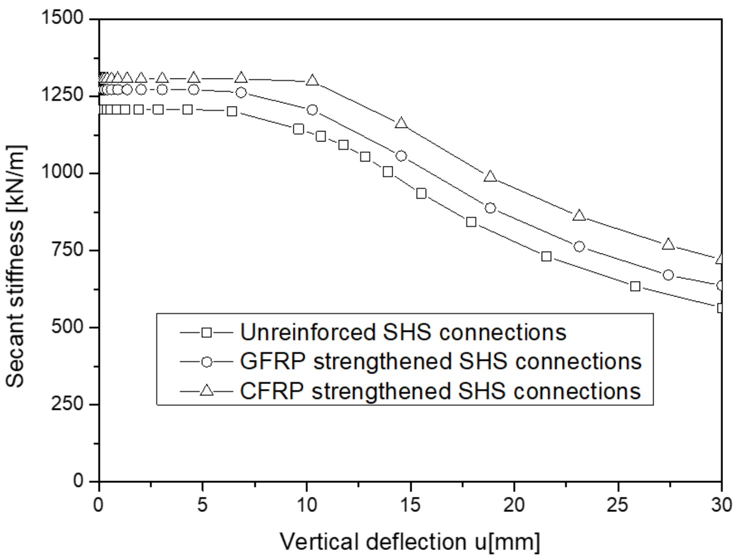

Figure 9. Secant stiffnesses versus displacements for the connections under static loading.

4.2. Under Cyclic Loading

Figure 10, representing the evolutions of the force-displacement hysteresis loops as a function of the number of loading cycles, give a first overview of the evolution of the elastoplastic behaviour of the un-strengthened connection under cyclic loading. Figure 10a compares the response under a single loading cycle to the static response. The first part of the curve corresponding to the cyclic loading coincides with the monotonic response. Unloading takes place in a parallel path to that of the initial stiffness of the connection. The total response, force-displacement, displays an identical behaviour in tension and compression. These first observations also confirm the isotropy of the elastoplastic behaviour of the steel material during cyclic loading. Figure 10b shows two loading cycles. The force-displacement curves display isotropic hardening as they have the same centre.

Based on these remarks, it can be stated that the first two cycles correspond to the transient phase. Beyond two loading cycles, a certain stability of the response is observed, where the envelope does not change in size as clearly shown in Figure 10c obtained under seven cycles of loading. The same observations can be made in the case of the strengthened connections.

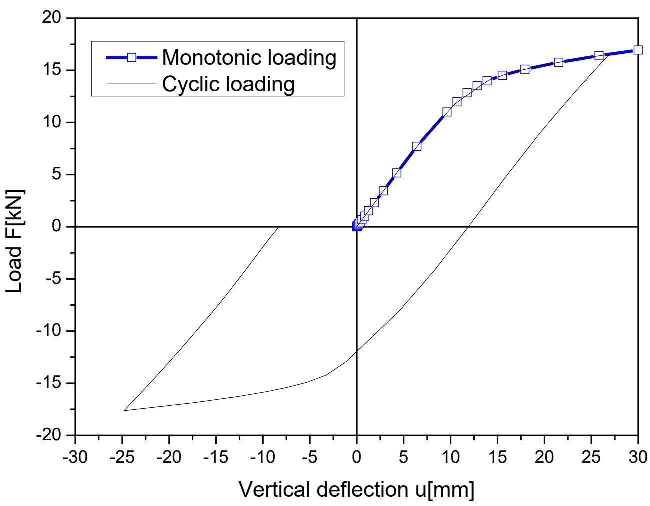

(**a**) One cycle

Figure 10. *Cont.*

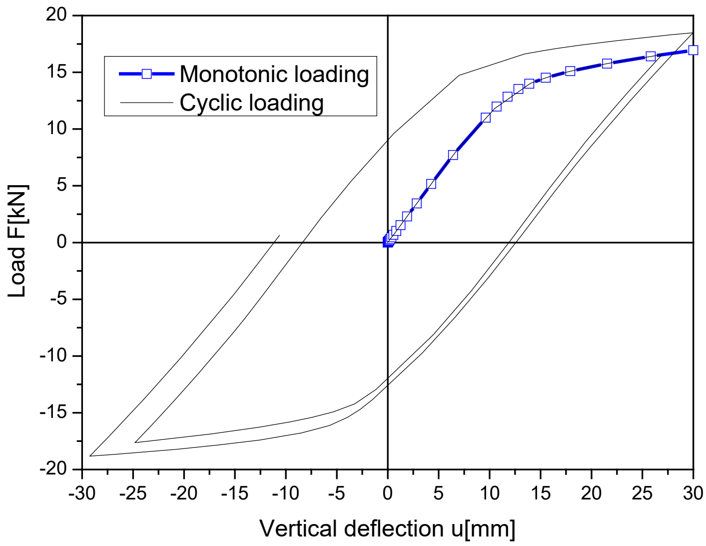

(**b**) Two cycles

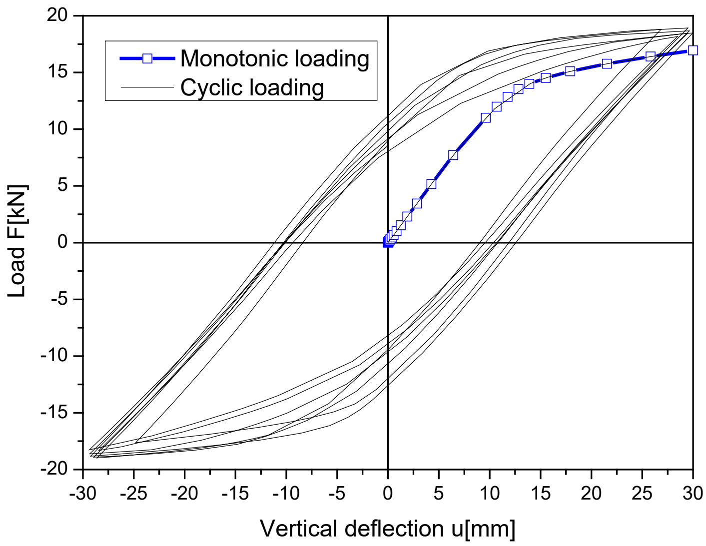

(**c**) Seven cycles

Figure 10. Force displacement curves under cyclic loading.

5. Parametric Study

The previous simulations have shown that the numerical model can predict the mechanical response of steel connections strengthened with FRPs under monotonic and cyclic loading. In what follows, the model will be used to study the response of connections made of different profiles. In Europe, and particularly in France, the use of I-shaped profiles is very common in steel construction, hence the interest in studying their behaviour under cycling loading.

The connection shown in Figure 11, consisting of welded I profile (IPE200), is analysed using the same material properties as previously described. The finite element model consists of 8000 solid elements type C3D8.

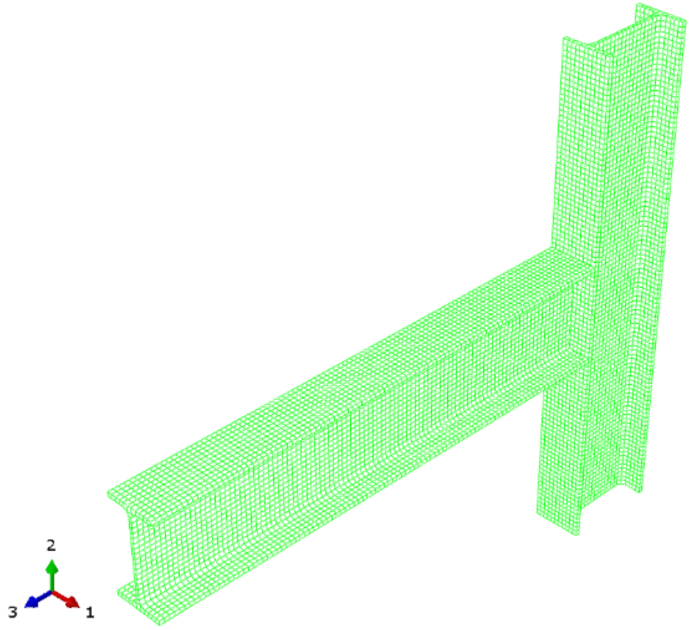

Figure 11. Finite element model of a non-strengthened connection consisting of IPE 200.

Figure 12 shows the distribution of the von Mises stress corresponding at a vertical displacement u = 20 mm. It clearly shows an area of stress concentration $\sigma_y = 804.2$ MPa at the extreme fibres of the beam at the level of the weld fillets. In general, if the vertical displacement is important, there can be a local buckling of the column web.

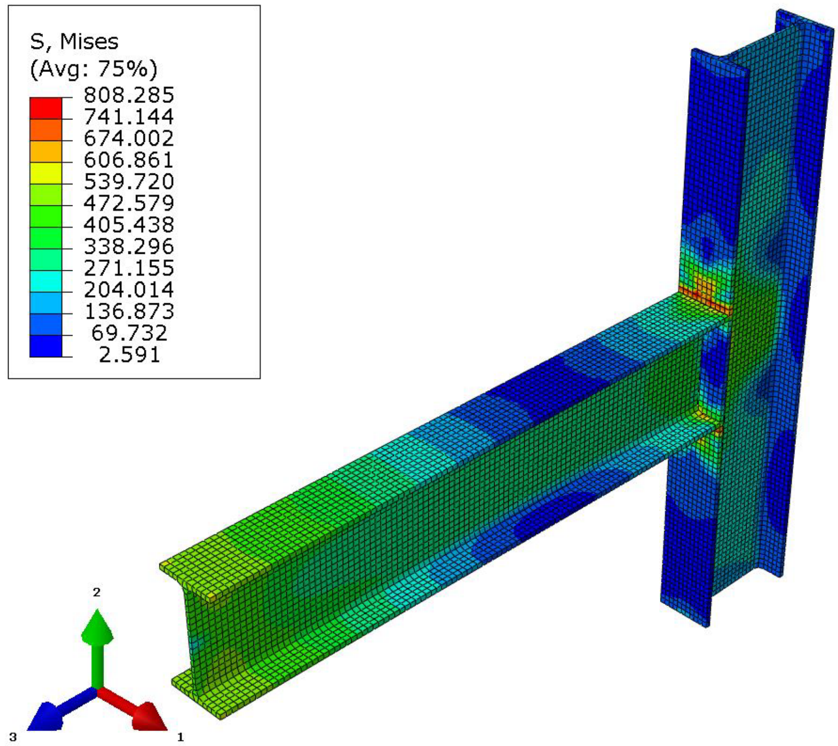

Figure 12. Contour plot of the von Mises stress under monotonic loading for the unstrengthened connection.

To avert any buckling; it is proposed to strengthen the connection as shown in Figure 13.

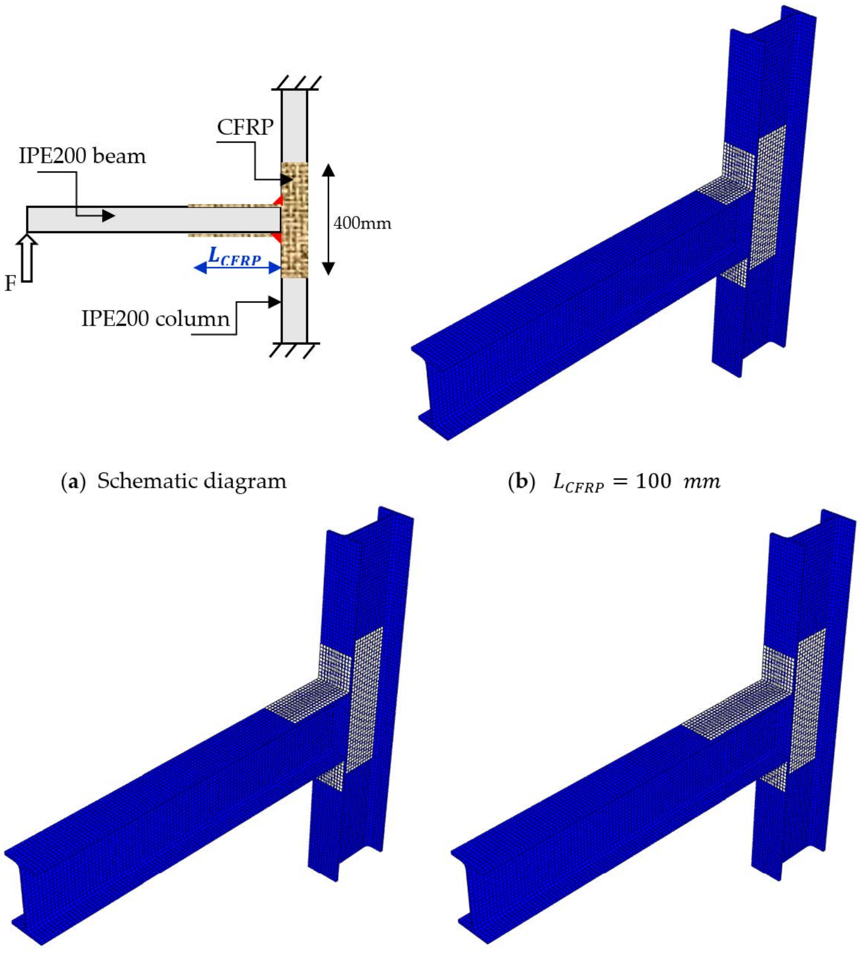

(**a**) Schematic diagram (**b**) $L_{CFRP} = 100\ mm$

(**c**) $L_{CFRP} = 200\ mm$ (**d**) $L_{CFRP} = 300\ mm$

Figure 13. Strengthening scheme for the connection.

The CFRP laminates are modelled with shell elements, type S4, of size 10 mm. The results of the simulations in terms of the von Mises stress, corresponding to a vertical displacement of the beam of approximately u = 20 mm, are shown on Figure 14.

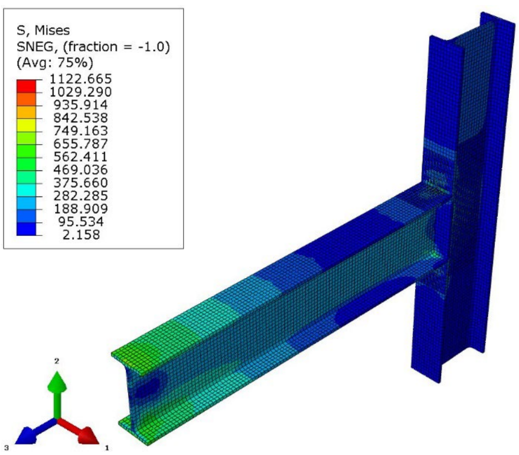

(**a**) $L_{CFRP} = 100\ mm$

Figure 14. *Cont*.

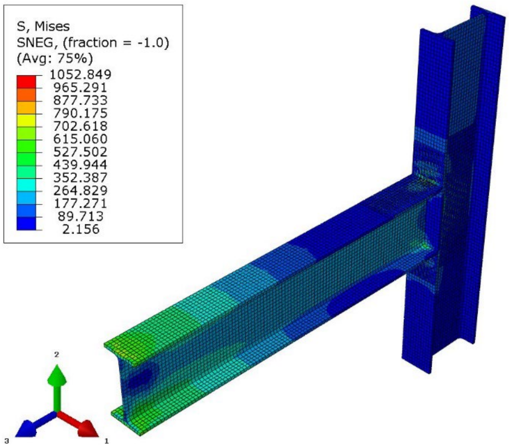

(**b**) $L_{CFRP} = 200\ mm$

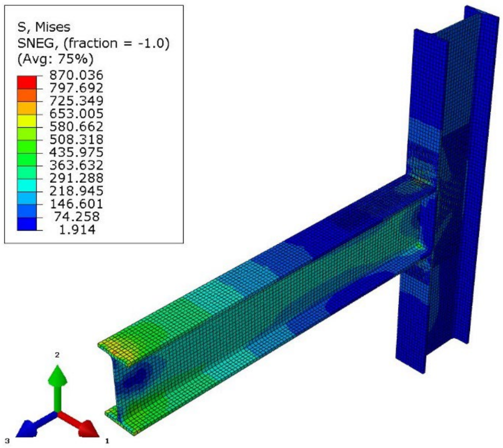

(**c**) $L_{CFRP} = 300\ mm$

Figure 14. Contour plot of the von Mises stress as a function of the strengthening length L_{CFRP}.

To further investigate the effect of the lengths of the reinforcement, the results of three simulations with $L_{CFRP} = 100$, 200 and 300 mm, are compared with those of the unstrengthened connection for a single loading cycle as shown in Figure 15. Quantitatively, all the numerical models lead to the same answers: strengthening a connection with I-sections is not as effective as strengthening a connection with square hollow sections (SHS).

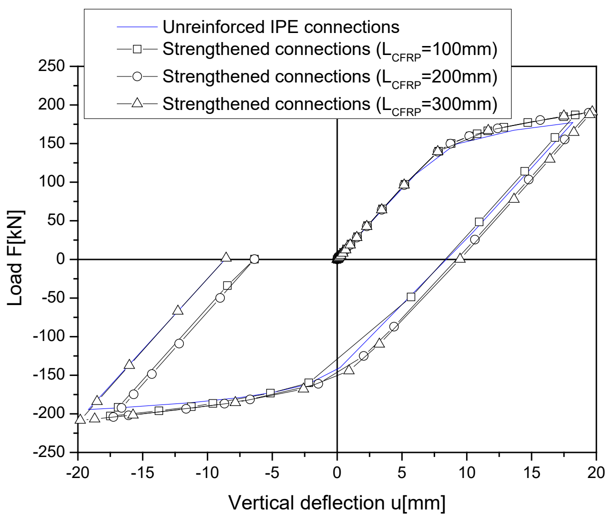

Figure 15. Force displacement curves for one loading cycle ($L_{CFRP} = 100$ mm).

6. Conclusions

The failure of a steel structure is primarily the result of a connection failure. A numerical approach for the analysis of strengthened steel connections under monotonic and cycling loading is therefore developed and presented. A beam column connection was chosen for this purpose because it the most widely used type of connection. The behaviour of the connection was simulated both under monotonic and cyclic loadings. The adhesive is modelled using the cohesive zone model available in Abaqus. In general, a good agreement was observed between the simulated load-displacement curves and the experimental results. Furthermore, the capture of the loading-unloading paths contributed to the understanding and explaining of the hysteresis phenomena observed during the cyclic behaviour. The most significant points of this contribution can be summarised as follows:

1. Numerical modelling of the cyclic behaviour of FRP strengthened steel connections is rarely presented in the literature compared to other civil engineering structures such as reinforced concrete and timber structures.
2. The developed numerical procedure complements the experimental work of Tafsirojjaman et al. [1];
3. The parametric analysis revealed that strengthening a connection with I-sections is not as effective as strengthening a connection with square hollow sections (SHS). In the latter, a simple bonding of a 0.6 mm thick CFRP laminate resulted in a considerable increase in the capacity of the connection; that is: an improvement of 14.85% in mechanical resistance using GFRP and 27% using CFRP.

Author Contributions: Simulation, M.K.; validation, M.K., A.K. and M.O.; original draft preparation, M.K.; conceptualisation, A.K.; redaction, A.K.; review, A.K.; editing, A.K.; methodology, M.O. All authors have read and agreed to the published version of the manuscript.

Funding: This research has received no funding.

Institutional Review Board Statement: Not applicable.

Informed Consent Statement: Not applicable.

Data Availability Statement: Not applicable.

Conflicts of Interest: The authors declare no conflict of interest.

References

1. Tafsirojjaman, T.; Fawzia, S.; Thambiratnam, D.; Zhao, X.-L. Behaviour of CFRP strengthened CHS members under monotonic and cyclic loading. *Compos. Struct.* **2019**, *220*, 592–601. [CrossRef]
2. Tafsirojjaman, T.; Fawzia, S.; Thambiratnam, D.P.; Zhao, X.-L. FRP strengthened SHS beam-column connection under monotonic and large-deformation cyclic loading. *Thin-Walled Struct.* **2021**, *161*, 107–518. [CrossRef]
3. Khelifa, M.; Celzard, A.; Oudjene, M.; Ruelle, J. Experimental and numerical analysis of CFRP-strengthened finger-jointed timber beams. *Int. J. Adhes. Adhes.* **2016**, *68*, 283–297. [CrossRef]
4. Alhamdan, Y.; Dirikgil, T. Experimental Investigation of the Flexural Strengthening of Fixed-Supported RC. *Int. J. Civ. Eng.* **2020**, *18*, 1229–1246. [CrossRef]
5. Hu, L.; Feng, P.; Zhao, X.L. Fatigue design of CFRP strengthened steel members. *Thin-Walled Struct.* **2017**, *119*, 482–498. [CrossRef]
6. Siddique, M.A.A.; El Damatty, A.A.; El Ansary, A.M. A numerical investigation of over strength and ductility factors of moment resisting steel frames retrofitted with GFRP plates. *Can. J. Civ. Eng.* **2014**, *41*, 17–31. [CrossRef]
7. Feng, P.; Hu, L.; Zhao, X.-L.; Cheng, L.; Xu, S. Study on thermal effects on fatigue behavior of cracked steel plates strengthened by CFRP sheets. *Thin-Walled Struct.* **2014**, *82*, 311–320. [CrossRef]
8. Bambach, M.R.; Elchalakani, M. Plastic mechanism analysis of steel SHS strengthened with CFRP under large axial deformation. *Thin-Walled Struct.* **2007**, *45*, 159–170. [CrossRef]
9. Wang, M.; Shi, Y.; Wang, Y.; Shi, G. Numerical study on seismic behaviors of steel frame end-plate connections. *J. Constr. Steel Res.* **2013**, *90*, 140–152. [CrossRef]
10. Fryba, L.; Urushadze, S. Improvement of fatigue properties or orthotropic decks. *Eng. Struct.* **2011**, *33*, 1166–1169. [CrossRef]
11. Si Larbi, A.; Ferrier, E.; Jurkiewiez, B.; Hamelin, P. Static behaviour of steel concrete beam connected by bonding. *Eng. Struct.* **2007**, *29*, 1034–1042. [CrossRef]
12. Teng, J.G.; Yu, T.; Fernando, D. Strengthening of steel structures with fiber-reinforced polymer composites. *J. Constr. Steel Res.* **2012**, *78*, 131–143. [CrossRef]

13. Bui, T.Q.; Hu, X. A review of phase-field models, fundamentals and their applications to composite laminates. *Eng. Fract. Mech.* **2021**, *248*, 107705. [CrossRef]
14. Cao, Y.; Cao, Z.; Zhao, Y.; Zuo, D.; Tay, T.E. Damage progression and failure of single-lap thin-ply laminated composite bolted joints under quasi-static loading. *Int. J. Mech. Sci.* **2020**, *170*, 105360. [CrossRef]
15. Zhang, P.; Yao, W.; Hu, X.; Bui, T.Q. 3D micromechanical progressive failure simulation for fiber-reinforced composites. *Compos. Struct.* **2020**, *249*, 112534. [CrossRef]
16. Yin, B.B.; Zhang, L.W. Phase field method for simulating the brittle fracture of fiber reinforced composites. *Eng. Fract. Mech.* **2019**, *211*, 321–340. [CrossRef]
17. Ülger, T.; Sharifi, A.S. Numerical Performance Analysis of Concrete-Filled Hollow GFRP Beams including Inner Surface Bearing Stresses at the Interface. *Buildings* **2022**, *12*, 1340. [CrossRef]
18. *Abaqus* Dassault Systèmes Simulia Corp: Providence, RI, USA. 2020. Available online: https://www.3ds.com/products-services/simulia/products/abaqus/ (accessed on 16 August 2022).
19. Khelifa, M.; Vila Loperena, N.; Bleron, L.; Khennane, A. Analysis of CFRP strengthened timber beams. *J. Adhes. Sci. Technol.* **2014**, *28*, 1–14. [CrossRef]
20. Hill, R. A new method for determining the yield criterion and plastic potential of ductile metals. *J. Mech. Phys. Solids.* **1953**, *1*, 271–276. [CrossRef]